Continuous Band-Filling Control and One-Dimensional Transport in Metallic and Semiconducting Carbon Nanotube Tangled Films

Hidekazu Shimotani, Satoshi Tsuda, Hongtao Yuan, Yohei Yomogida, Rieko Moriya, Taishi Takenobu, Kazuhiro Yanagi, and Yoshihiro Iwasa*

Field-effect transistors that employ an electrolyte in place of a gate dielectric layer can accumulate ultrahigh-density carriers not only on a well-defined channel (e.g., a two-dimensional surface) but also on any irregularly shaped channel material. Here, on thin films of 95% pure metallic and semiconducting single-walled carbon nanotubes (SWNTs), the Fermi level is continuously tuned over a very wide range, while their electronic transport and absorption spectra are simultaneously monitored. It is found that the conductivity of not only the semiconducting but also the metallic SWNT thin films steeply changes when the Fermi level reaches the edges of one-dimensional subbands and that the conductivity is almost proportional to the number of subbands crossing the Fermi level, thereby exhibiting a one-dimensional nature of transport even in a tangled network structure and at room temperature.

1. Introduction

Controlling charge-carrier density is of vital importance for investigating properties and creating new functions of materials. Various chemical methods such as impurity doping, element substitution and intercalation have been used for this purpose. Among the various methods, field-effect transistors (FETs) have attracted growing interest because of their continuous and reversible controllability for carrier densities. However, FETs have a limitation in that the carrier density they accumulate is always less than 10^{13} cm^{-2}. Recently, a new method, sometimes called electric double layer transistor (EDLT), has been developed as a powerful carrier density control method, which combines the advantages of FETs with ability for high density carrier control. EDLT employs an electrolyte as the gate dielectric layer instead of using a solid insulating layer such as SiO_2 in conventional FETs, enabling high density carrier accumulation over 10^{14} cm^{-2}. With this technique on such solid matter as organic semiconductors,[1–7] carbon nanotubes,[8–15] graphene,[19] oxides,[20–27] and inorganic layered materials,[28–30] various interesting phenomena such as field-induced superconductivity[28,30] and ferromagnetism[26] have been reported, which were impossible with conventional transistors. In particular, many studies have been carried out on single-walled carbon nanotubes (SWNTs) using the electrolyte-gating method because of the high electrochemical stability. For example, its strong gate coupling enabled carrier injections of both electron and hole to SWNT thin film by applying a small gate voltage, and near-infrared light emission from the film was demonstrated.[12] This demonstrates that the electrolyte-gating method is suitable to control both electron and hole density in SWNTs in a wide range. The high density control of electrons and holes greatly changes absorbance of SWNTs. The electromodulated transmittance of SWNT films have been studied from the viewpoint of optoelectronic application such as electrochromic smart windows from far-infrared to visible light.[31,32] In addition to the practical viewpoint, the change in the absorbance of SWNTs are useful to detect degrees of subband fillings. Such an optical detection of band filling of EDLT channel has been employed for nanocrystal thin films[16] such as PbSe[17] and CdSe.[18]

One-dimensional transport in SWNTs, such as Tomonaga–Luttinger liquid behavior, is of great interest from the viewpoint of fundamental physics and has already been investigated intensively. However, quantized transport reflecting the multi-subband electronic structure of SWNTs has not yet been clearly observed because it requires a wide range of Fermi level tuning combined with in-situ detection of the subband filling. In particular, any substantial resistivity changes of FETs of metallic SWNTs proportional to the number of current carrying subband, which are expected from one-dimensionality of SWNTs, have not been reported yet. In individual SWNT FETs, optical detection of subband filling is impossible. Although the use

Dr. H. Shimotani, S. Tsuda, Dr. Y. Yomogida
Department of Physics
Tohoku University
Sendai, Miyagi, 980–8578, Japan
E-mail: Shimotani@sspns.phys.tohoku.ac.jp
Dr. H. T. Yuan, Prof. Y. Iwasa
Quantum-Phase Electronics Center
The University of Tokyo
Tokyo, 113–8656, Japan
R. Moriya, Dr. K. Yanagi
Department of Physics
Tokyo Metropolitan University
Hachioji, Tokyo, 192–0397, Japan
Prof. T. Takenobu
Department of Applied Physics, Waseda University
Shinjyuku, Tokyo, 169–8050, Japan

DOI: 10.1002/adfm.201303566

of SWNT thin film is appropriate for detecting subband filling with optical absorption spectroscopy,[33] and capacitance measurements, a conventional SWNT film, which is a mixture of metallic and semiconducting SWNTs, hinders observations of intrinsic transport properties. To overcome these obstacles, we employed an EDLT configuration to tune the Fermi level of SWNTs over a wide range, and used a separated semiconducting and metallic SWNT thin film of more than 95% purity as an active channel to measure its absorption spectra.

Here we report the continuous tuning of the Fermi level over 2 eV owing to the huge density carrier accumulation in the separated metallic and semiconducting SWNT thin films and the in-situ measurements of the subband fillings and conductivities. We successfully observed a stepwise increase of the conductivity associated with spectral evolutions both in metallic and semiconducting SWNT thin films, which is a manifestation of the one-dimensional nature of transport even in a tangled network structure.

2. Results and Discussion

The conductance of a semiconducting and metallic SWNT thin-film was measured by a four-terminal method while controlling the Fermi level in an electrochemical cell (**Figure 1**). Because carrier doping in EDLTs of SWNT films has characteristics of electrochemical doping to some extent, we call the transistor an electrochemical transistor (ECT) in a wider sense. A typical transfer characteristic (source–drain current I_D vs gate voltage V_G) of ECTs based on a semiconducting SWNT thin film is plotted in **Figure 2**a. For the precise control of the electrochemical potential of the SWNT thin films, we used a Ag|Ag$^+$ reference electrode, and the gate voltage (V_G) is defined as the potential of the reference electrode with respect to the SWNT film. We observed a relatively large hysteresis in the semiconducting SWNT ECT (see Supporting information). For simplicity, only a partial transfer curve was plotted. Owing to the strong gate coupling of ECTs, the on/off ratio of the transistor was as high as 1×10^4 (Figure 2a), which, compared with conventional SWNT FETs, is significantly large when taking the film thickness (300 nm) into account. The conductance of the semiconducting SWNT thin-film ECT has a minimum at $V_G = 0.9$ eV and showed symmetric ambipolar behavior with a wavy increase of I_D. The transconductance ($g_m = |dI_D/dV_G|$) is plotted against V_G in Figure 2b.

The transfer characteristics of an ECT on a metallic SWNT thin film in Figure 2c showed steep increases in conductance by both electron and hole doping and the large on/off ratio of 5.6, which is remarkably large as a transistor response of metallic SWNTs. Another noticeable feature of the transfer curve of the metallic SWNT thin film ECT is the dip at $V_G \approx 0.8$ V, which corresponds to the charge neutrality point considering that the M_{11} absorption peak has maximum intensity at $V_G = 0.8$ V as described later. A similar conductivity dip was reported for a SiO_2 gated field-effect transistor of an individual metallic SWNT,[34] which is attributable to strong isolated defects on the basis of theoretical investigations.[35] In a marked contrast with the considerable hysteresis in the semiconducting SWNT ECTs, the I_D–V_G curve in the metallic SWNT shown in Figure 2c is almost hysteresis-free, a finding of great help in understanding the transport mechanism related to the band structure and subband filling. The transconductance is plotted against V_G in Figure 2d.

As a powerful tool to confirm the subband filling in the highly charged SWNT film, an optical absorption spectroscopy measurement (Figure 1b) was simultaneously performed with the transport measurement. **Figure 3**a shows the spectral variation of the semiconducting SWNT films upon electron (top panel) and hole (bottom panel) doping. The semiconducting SWNT film showed two distinct absorption peaks at 1830 and

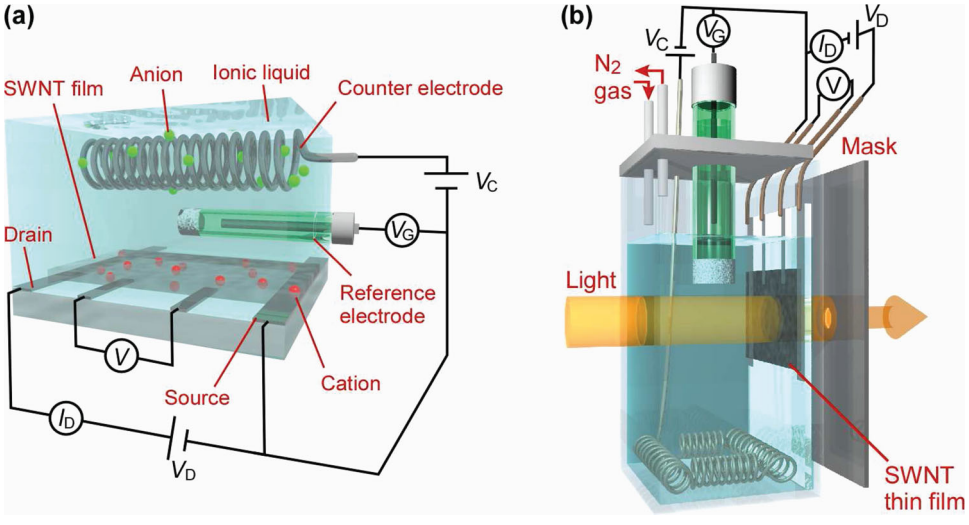

Figure 1. a) Measurement configuration of the electrochemical transistor of SWNT thin films. Carrier density of the SWNT film was changed by applying voltage (V_C) to the counter electrode. The gate voltage applied to the SWNT film (V_G) was controlled with a Ag/Ag$^+$ reference electrode. The conductance of the film was measured by the four-terminal method, applying a source–drain voltage (V_D) of 50 mV. b) Schematic diagram of simultaneous measurements of transistor characteristics and optical absorption spectra. Light was irradiated to the semiconducting SWNT thin film installed in the quartz cell, and the light beam was narrowed by a mask to remove the effect of electrodes.

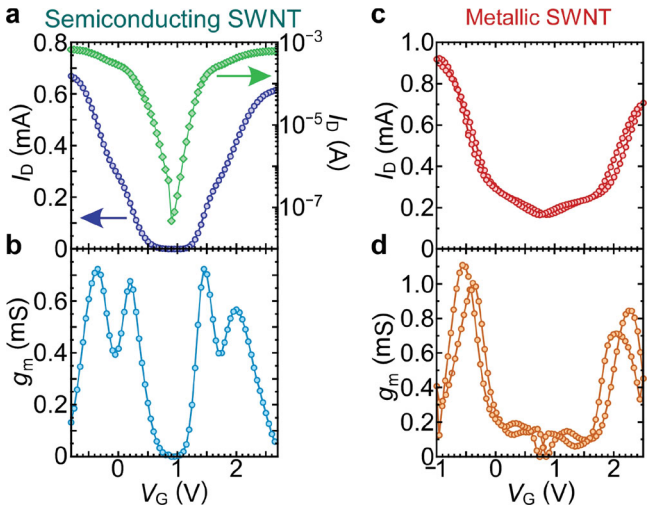

Figure 2. a) Drain current (I_D) vs gate voltage (V_G) plots of the semiconducting SWNT thin film. Only the curves from both ends of the gate voltage to the point of minimum drain current are shown hereinafter for clarity. Blue circles and green diamonds show the same data in linear and logarithmic scales, respectively. b) Transconductance (g_m) of the semiconducting SWNT thin film plotted against V_G. c) I_D vs V_G curve of a metallic SWNT thin film. d) g_m of the metallic SWNT film plotted against V_G.

1010 nm. These absorptions correspond to electronic transition from the first valence subband to the first conducting subband (S_{11}) and from the second valence subband to the second conducting subband (S_{22}), respectively. Sharp peaks around 1700 and 1900 nm are from the ionic liquid. By comparing the contour map of absorption spectra plotted against V_G (Figure 3b) with a transfer curve shown in Figure 3c for the semiconducting SWNT thin film, we found that the bleaching of the two absorption peaks coincides with the conductivity increase in the semiconducting SWNT ECT. The conductivity of the film increased from the off state when the S_{11} peak started to decrease, and it came close to saturation when the S_{11} peak disappeared in both cases of electron and hole doping, while the conductivity increased again when the S_{22} peak decreased and came close to saturation when the S_{22} peak disappeared.

Similar behavior was also observed for the metallic SWNT thin-film ECT. The absorption peak at 710 nm in the spectra of the metallic SWNT thin film shown in **Figure 4**a corresponds to the electronic transition from the first valence subband to the first conducting subband (M_{11}). Figure 4a shows that the M_{11} absorbance was decreased by both electron (top panel) and hole (bottom panel) doping, which is similar to the previous report using electrochemical doping.[36] Similar to the case in the semiconducting SWNT film, the intensity modulation of the absorption band coincided with the conductivity change of the metallic SWNT film shown in Figure 4c.

Here, we discuss the transfer curves of both semiconducting and metallic SWNT thin-film ECT showing stepwise changes in conductance by both hole and electron doping, as shown in Figure 2a,c. In particular, different from the conventional FET with solid gate dielectrics that cannot modulate the conductance of metallic SWNTs, the on/off ratio of 5.6 in Figure 2c is remarkably large for metallic SWNTs, which are directly related with the strong gate coupling in ECT.

The conductance of the semiconducting SWNT thin-film ECT has a minimum at V_G = 0.9 eV and showed two steep increases, from V_G = 0.5 to 0.2 eV and from V_G = –0.1 to –0.5 eV by hole doping, and two steep increases, from V_G = 1.3 to 1.6 eV and from V_G = 1.9 to 2.2 eV for electron doping. The stepwise increase in the drain current is more noticeable as a peak in the plot of the transconductance vs the gate voltage (Figure 2b). Similar steep increases in the conductance of SWNTs were

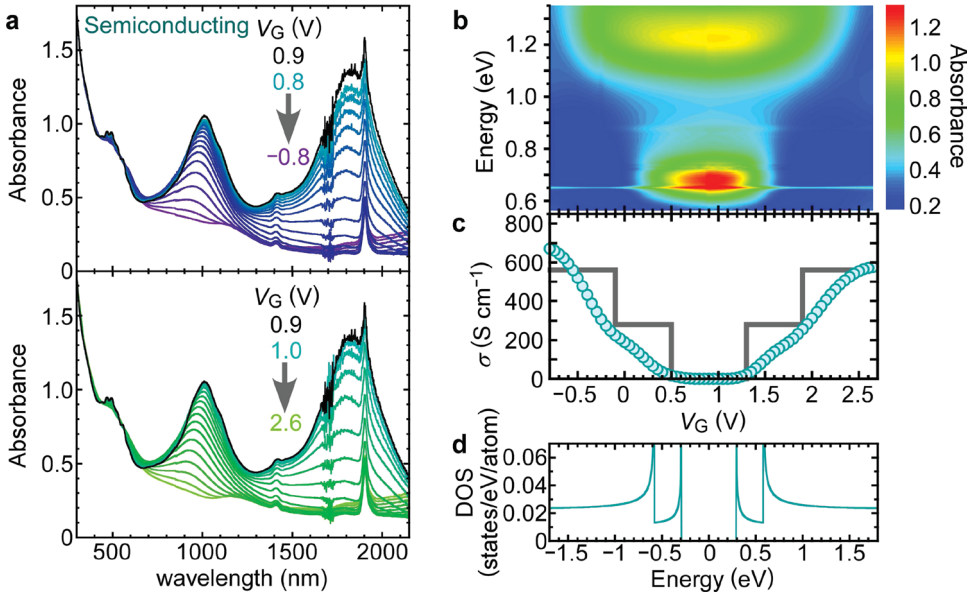

Figure 3. a) Absorption spectra measured at various gate voltages (V_G). b) Contour map of absorbance as a function of the energy of the light and V_G. c) Conductivity (σ) plotted against V_G. The grey line is a visual guide showing the stepwise increase of the conductivity. d) Schematic diagram of density of states (DOS) of a semiconducting SWNT of (17,3) chirality index.

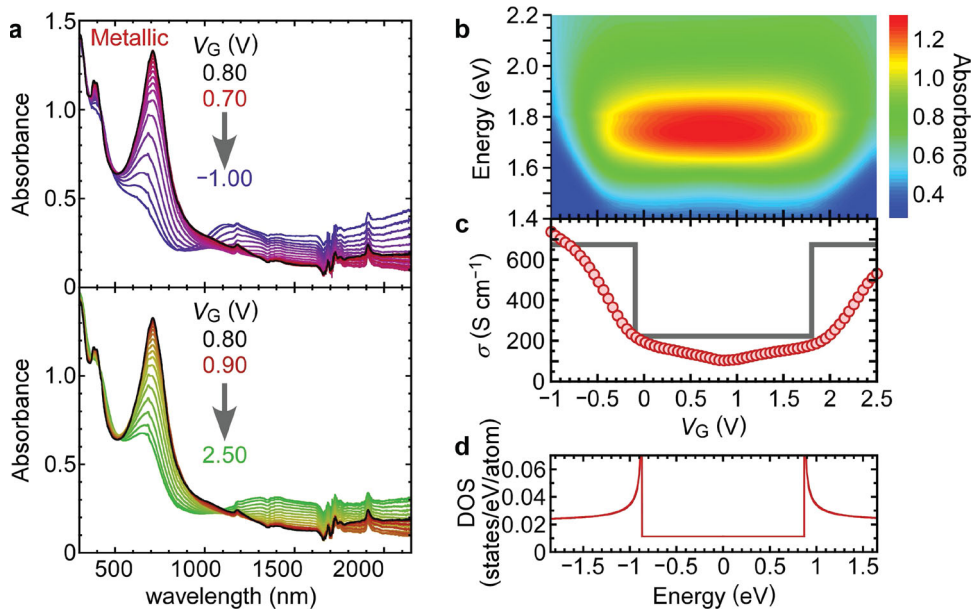

Figure 4. a) Absorption spectra measured at various gate voltages (V_G). b) Contour map of absorbance as a function of the energy of the light and the gate voltage. c) Conductivity plotted against the gate voltage. The grey line is a visual guide showing the stepwise increase of the conductivity. d) Schematic diagram of density of states (DOS) of a metallic SWNT of (15,6) chirality index.

observed in the metallic-SWNT thin-film ECT, from −0.3 to −0.7 eV by hole doping and from 2.0 to 2.4 eV by electron doping. According to the Landauer formula, the conductance of a one-dimensional conductor is proportional to the number of current-carrying subbands.[37]

By employing SWNT thin films as active layers, the subband fillings discussed above can be directly observed by absorption spectroscopy. Figure 3a shows that both the S_{11} and S_{22} absorption bands have maximum absorbance at $V_G = 0.9$ eV, indicating that $V_G = 0.9$ eV is the charge neutrality point. Upon both electron and hole doping with ionic liquid gating, the S_{11} peak disappeared first, followed by the S_{22} peak as the carrier density increased. This means the first and second subbands were sequentially filled by changing V_G from the charge neutrality point. One can clearly see such kind of features in the V_G-dependent absorption spectra, plotted in the form of a contour map in Figure 3b.

By comparing the contour map with the transfer curve in Figure 3c, it is concluded that the first and second steep increases in the conductivity are ascribed to the shift of the Fermi level from inside the band gap to the first and second subband, respectively, for both electron and hole doping. By shifting the Fermi level from the charge neutrality point at $V_G = 0.9$ V to the first subband and then the second subband, the number of current-carrying subbands changes from 0 to 2 and then to 4.[38] In an ideal one-dimensional ballistic conductor, the dependence of conductivity on subband filling is proportional to the number of subbands, as indicated by the grey line in Figure 3c. It is noteworthy that even in such tangled SWNTs as these randomly connected thin films, the transport characteristics still show a pure and clear one-dimensional conductance. A similar study was reported for CdSe nanocrystal solids, where the conductivity has a peak around half-filling of the lowest conduction band quantum state.[39] This is contrasting to the present result of the stepwise monotonous increase in the conductivity of the SWNT thin film. The difference is a consequence of the difference in dimensionality of nanomaterials constituting the films.

Like semiconducting SWNT thin film, the variation in absorption spectra with V_G shown in Figure 4a indicates that $V_G = 0.8$ V is the charge neutrality point of the metallic SWNTs and that both the first conducting and valence subband can be filled by the ECT. The conductivity of the metallic SWNT thin film increased from the off state when the M_{11} peak decreased and became saturated when the M_{11} peak disappeared, suggesting that the increase in the conductivity of the metallic SWNT thin film can be attributed to the increase in the number of subbands available for transport, here specifically, say, from two to six subbands, considering the degeneracy of the bands.[38] The grey line (for visual guidance) in Figure 4c indicates the conductivity ratio of two to six, which is quantitatively in accord with the on/off ratio of the measured conductivity. Therefore, the considerably large on/off ratio of about 5.6 in the transfer characteristic of the metallic SWNT thin-film ECT arises quantitatively originates from the further shift of the Fermi level up/down to the first conducting or valence multiband filling, which has never been reported with use of conventional FETs.

Figure 3d shows the energy dependence of the density of states for the semiconducting SWNT with a diameter of 1.46 nm, which is the average diameter of SWNTs obtained by the same preparation method.[40] The density of states was calculated with zone-folding tight-binding calculations.[38] The nearest-neighbor carbon-carbon tight-binding overlap energy and distance employed in the calculations were 3.0 eV and 0.142 nm, respectively.[41] The calculated S_{11} and S_{22} band gaps are 0.583 eV and 1.17 eV, which are smaller than corresponding optical band gaps of 0.678 eV and 1.23 eV, respectively, obtained from the absorption spectrum at $V_G = 0.9$ V. These discrepancies are explained by a blue shift of the absorption bands because of an electron-electron interaction, which is larger

than a red shift because of an excitonic effect,[42] and generally observed in particular for the S_{11} absorption.[41]

As shown in Figure 3b, the V_G gap (around 0.8 V) between the first steep increases of the conductivity by electron/hole doping is larger than the S_{11} band gap of 0.583 eV by only 0.12 eV. In sharp contrast, the second V_G gap between the steep increase in the conductivity seen at V_G = 1.9 V and –0.1 V for electron and hole doping, respectively, is larger than the calculated S_{22} band gap of 1.17 eV by 0.73 eV. This contrasting behavior of S_{11} and S_{22} can be explained by considering a serial connection of geometrical and quantum capacitances. The geometrical capacitance is determined by the geometrical configuration of the whole film and the dielectric constant of the dielectric layer, whereas the quantum capacitance is proportional to the density of states. When E_F is within the band gap, the density of states is extremely small, which means that the quantum capacitance dominates the total capacitance. In such a case, the applied V_G directly shifts E_F. This explains the fact that the S_{11} gap in the conductivity coincides with the calculated S_{11} band gap. This kind of direct measurements of a band gap with ECT has been reported for organic semiconductors in the EDLT configuration.[43]

On the other hand, the shift of Fermi level from the first subband to the second subband, which is 0.29 eV from the calculation, requires the V_G change of 0.6 V [= (2.0 – 0.8)/2 V]. The result indicates that the 0.6 V of the V_G change is divided into 0.29 V for the quantum capacitance and 0.31 V for the geometrical capacitance. This means that the quantum capacitance is comparable with the geometrical capacitance when the Fermi level reaches the first valence or conducting subband.

In the metallic SWNTs, the gap (≈1.9 V) between the threshold voltages of the sharp increases of the conductivity is slightly larger than the calculated M_{11} band gap of 1.74 eV. This means the voltage is divided into 1.74 V for the quantum capacitance and 0.16 V for the geometrical capacitance. The quantum capacitance is finite as expected from the finite density of states (Figure 4d) between the first valence and the conducting subbands in metallic SWNTs. Because of this finite quantum capacitance inside the M_{11} gap, a higher V_G is required to shift E_F to touch the first valence or conducting subbands to increase conductivity than the V_G required in the semiconducting SWNTs. Only by employing ECT, which can vary the carrier density of the whole film over a much wider range, could the conductivity of the metallic SWNTs be modulated.

The accumulated charge densities in the SWNT films were estimated by the capacitance measurements. **Figure 5**a and b shows the V_G dependences of the capacitances of the semiconducting and metallic SWNT films, respectively, obtained from ac impedance measurements. Both curves shows significant V_G dependences, which is symmetric about the charge neutral points, i.e., V_G = 0.9 and 0.8 V for the semiconducting and metallic SWNT film respectively. The behavior is explained by the V_G dependence of quantum capacitances, which are proportional to their density of states at the Fermi level. The two steep increases of the capacitance of the semiconducting SWNT films by both hole and electron doping are attributable to increases of the quantum capacitance by filling the first and second subband. To discuss about this, the derivatives of the peak area of absorption bands $|dA/dV_G|$ of the S_{11} and S_{22} transition of the

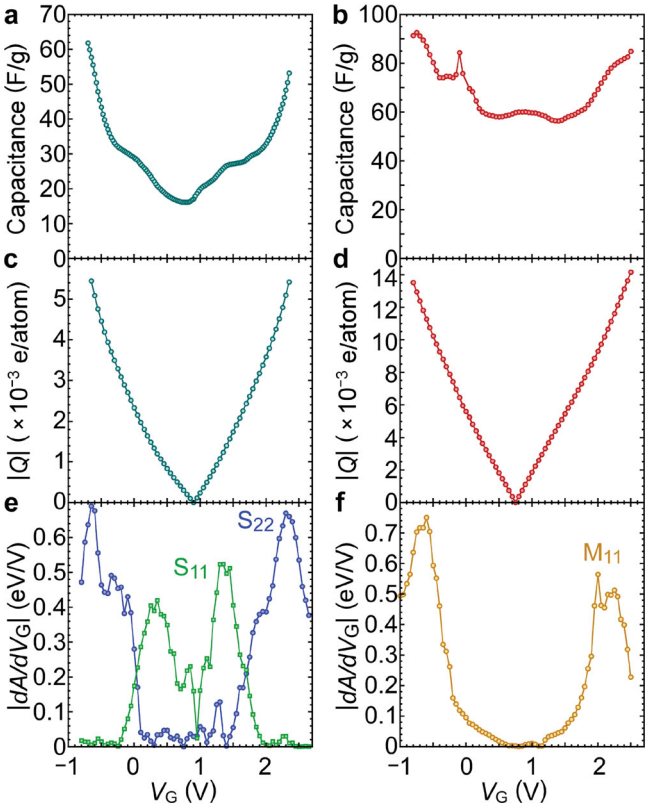

Figure 5. a,b) Capacitance of the semiconducting and metallic SWNT film, respectively, plotted against the gate voltage (V_G). c,d) Absolute value of accumulated charge density ($|Q|$) in the semiconducting and metallic SWNT film, respectively, plotted against V_G. e,f) The derivative of the peak area of absorption bands of the semiconducting and metallic SWNT film, respectively, with respect to V_G ($|dA/dV_G|$) plotted against V_G. The green squares, blue circles, and orange circles indicate S_{11}, S_{22}, and M_{11} transition, respectively.

semiconducting SWNT film are plotted against V_G in Figure 5e. The peak position of the derivatives, where the Fermi level is at a local maximum of the density of the states of the film owing to van Hove singularities, coincide with the V_G, where the capacitance steeply increases, as expected. Similarly, a comparison of Figure 5b and f indicates that the capacitance of the metallic SWNT film increases when the Fermi level reaches the first subband of SWNTs.

By integrating the capacitances with respect to the V_G, the amount of the charge in the SWNT thin films can be estimated (Figure 5c,d). The accumulated charge densities (Q) in the semiconducting SWNT thin film at V_G = 2.35 (electron) and –0.7 V (hole) are –44 and 47 C g^{-1}, which are equal to 0.0054 and 0.0058 e atom^{-1}, respectively. Also, those in the metallic SWNT thin film at V_G = 2.5 (electron) and –0.8 V (hole) are –114 and 109 C g^{-1}, which are equal to 0.0142 and 0.0135 e atom^{-1}, respectively. Q at the peaks of $|dA/dV_G|$ of S_{22} in Figure 5e are 0.0051 (electron) and 0.0054 (hole) e atom^{-1}. The values are comparable to the integration of the density of states of a semiconducting SWNT of 1.46 nm in diameter shown in Figure 3d from the charge neutral point to the second van Hove singularity (0.0057 e atom^{-1}). As in the case of the semiconducting SWNT thin film, Q at the

peaks of $|dA/dV_G|$ of the metallic SWNT thin film, which are 0.0093 (electron) and 0.0113 (hole) e atom^{-1}, are comparable to the integration of the density of states shown in Figure 4d from the charge neutral point to the first van Hove singularity (0.0099 e atom^{-1}).

3. Conclusion

By using ECTs with ionic liquid gating, we have reported simultaneous measurements of the conductivity and optical absorption spectra as well as capacitance measurements of separated semiconducting and metallic SWNT thin films by controlling E_F. By employing ECT, which can accumulate high carrier density, we realized clear multi-subband transport in both semiconducting and metallic SWNTs even in a tangled network structure. This is quite contrast to the conventional treatment of SWNT thin-film transistor, which assume semiconducting and metallic SWNT thin-film channel as two-dimensional conductor and gate-voltage independent conductor, respectively. The substantial change in the conductivity of the metallic SWNT thin film clearly shows that 1D transport characteristics of each SWNT strongly influence the transport characteristics of the SWNT thin film. It is also noteworthy that the multi-subband transports were observed at room temperature.

4. Experimental Section

Conductivity measurements on the semiconducting and metallic SWNT films were performed at room temperature under nitrogen flow. Semiconducting and metallic SWNTs were separated from as-prepared SWNTs with density gradient ultracentrifugation (DGU) method. The details for purification are described in ref.[40] Thin films of purified semiconducting and metallic SWNTs were fabricated on quartz substrates with four deposited platinum electrodes (50 nm in thickness). The full length, channel length, channel width and thickness of semiconducting SWNT film are 8.55 mm, 2.07 mm, 4.45 mm and 300 nm, respectively. Those of metallic SWNT films are 9.01 mm, 1.96 mm, 3.01 mm and 400 nm, respectively. The bulk density of the SWNT films was 0.29 g cm^{-3}. The SWNT thin film and a platinum wire serving as a counter electrode were installed in a quartz cell 1 cm wide and 1 cm thick (Figure 1a). Ionic liquid [*N*,*N*-dimethyl-*N*-methyl-*N*-(2-methoxyethyl)ammonium bis(trifluoromethanesulfonylimide), DEME-TFSI] purchased from Kanto Chemical was dried under vacuum at 120 °C overnight and poured into the cell as shown in Figure 1b. The cell was topped with a Teflon cap fitted with two Teflon tubes for a nitrogen gas inlet and outlet and a Ag|Ag$^+$ reference electrode. The reference electrode consisted of a silver wire and a 10 mM DEME-TFSI solution of silver trifluoromethanesulfonate as proposed in ref.[44] and connected to the cell through a glass frit. The carrier density and Fermi levels in SWNTs were controlled with an EDLT configuration by applying voltage between the platinum counter electrode and the SWNT thin film. The measurements of conductivity and control of the gate voltage were performed with an E5270A 8-Slot parametric measurement mainframe (Agilent Technologies). The absorption spectra were measured with a V-670 UV-Vis spectrophotometer (JASCO Corporation). The light beam was filtered by metal sheeting with a pinhole before detection to remove stray light. The capacitances of the SWNT films were calculated from ac impedances measured at 20 mHz for various V_G assuming an equivalent circuit of a capacitor and resistance in parallel. The ac impedance measurements were carried out with ZAHNER-elektrik IM6eX electrochemical workstation in an Ar glove box.

Supporting Information

Supporting Information is available from the Wiley Online Library or from the author.

Acknowledgements

H.S. was supported by JSPS KAKENHI Grants 23656011 and 24684023. K.Y. was supported by JSPS KAKENHI Grants 21108523 and 2365117. Y.I. was supported by a Grant-in-Aid for Specially Promoted Research (No. 25000003) and the FIRST Program from JSPS and SICORP from JST.

Received: October 18, 2013
Revised: December 16, 2013
Published online: February 12, 2014

[1] H. Shimotani, G. Diguet, Y. Iwasa, *Appl. Phys. Lett.* **2006**, *86*, 022104.
[2] J. Takeya, K. Yamada, K. Hara, K. Shigeto, K. Tsukagoshi, S. Ikehara, Y. Aoyagi, *Appl. Phys. Lett.* **2006**, *88*, 112102.
[3] M. J. Panzer, C. D. Frisbie, *Appl. Phys. Lett.* **2006**, *88*, 203504.
[4] H. Shimotani, H. Asanuma, J. Takeya, Y. Iwasa, *Appl. Phys. Lett.* **2006**, *89*, 203501.
[5] H. Shimotani, H. Asanuma, Y. Iwasa, *Jpn. J. Appl. Phys. Part 1* **2007**, *46*, 3613.
[6] T. Uemura, R. Hirahara, Y. Tominari, S. Ono, S. Seki, J. Takeya, *Appl. Phys. Lett.* **2008**, *93*, 263305.
[7] S. Ono, N. Minder, Z. Chen, A. Facchetti, A. F. Morpurgo, *Appl. Phys. Lett.* **2010**, *97*, 143307.
[8] M. Krüger, M. R. Buitelaar, T. Nussbaumer, C. Schönenberger, *Appl. Phys. Lett.* **2001**, *78*, 1291.
[9] S. Rosenblatt, Y. Yaish, J. Park, J. Gore, V. Sazonova, P. L. McEuen, *Nano Lett.* **2002**, *2*, 869.
[10] H. Shimotani, T. Kanbara, Y. Iwasa, K. Tsukagoshi, Y. Aoyagi, H. Kataura, *Appl. Phys. Lett.* **2006**, *88*, 073104.
[11] T. Ozel, A. Gaur, J. A. Rogers, M. Shim, *Nano Lett.* **2005**, *5*, 905.
[12] J. Zaumseil, X. Ho, J. R. Guest, G. P. Wiederrecht, J. A. Rogers, *ACS Nano* **2009**, *3*, 2225.
[13] J. Zhao, Y. Gao, W. Gu, C. Wang, J. Lin, Z. Chen, Z. J. Cui, *Mater. Chem.* **2012**, *22*, 20747.
[14] M. Ha, Y. Xia, A. A. Green, W. Zhang, M. J. Renn, C. H. Kim, M. C. Hersam, C. D. Frisbie, *ACS Nano* **2010**, *4*, 4388.
[15] W. Gomulya, G. D. Costanzo, E. J. F. de Carvalho, S. Z. Bisri, V. Derenskyi, M. Fritsch, N. Fröhlich, S. Allard, P. Gordiichuk, A. Herrmann, S Jan Marrink, M. C. dos Santos, U. Scherf, M. A. Loi, *Adv. Mater.* **2013**, *25*, 2948.
[16] D. Vanmaekelberg, A. J. Houtepen, J. J. Kelly, *Electrochim. Acta* **2007**, *53*, 1140.
[17] B. L. Wehrenberg, D. Yu, J. Ma, P. Guyot-Sionnest, *J. Phys. Chem. B* **2005**, *109*, 20192.
[18] S. C. Boehme, H. Wang, L. D. A. Siebbeles, D. Vanmaekelbergh, A. J. Houtepen, *ACS Nano* **2013**, *7*, 2500.
[19] J. T. Ye, M. F. Craciun, M. Koshino, S. Russo, S. Inoue, H. T. Yuan, H. Shimotani, A. F. Morpurgo, Y. Iwasa, *Proc. Natl. Acad. Sci. U. S. A.* **2011**, *108*, 13002.
[20] H. Shimotani, H. Asanuma, A. Tsukazaki, A. Ohtomo, M. Kawasaki, Y. Iwasa, *Appl. Phys. Lett.* **2007**, *91*, 082106.
[21] H. Shimotani, H. Suzuki, K. Ueno, M. Kawasaki, Y. Iwasa, *Appl. Phys. Lett.* **2008**, *92*, 242107.
[22] H. T. Yuan, H. Shimotani, A. Tsukazaki, A. Ohtomo, M. Kawasaki, Y. Iwasa, *Adv. Funct. Mater.* **2009**, *19*, 1046.

[23] K. Ueno, H. Shimotani, Y. Iwasa, M. Kawasaki, *Appl. Phys. Lett.* **2010**, *96*, 252107.
[24] S. Asanuma, P.-H. Xiang, H. Yamada, H. Sato, I. H. Inoue, H. Akoh, A. Sawa, K. Ueno, H. Shimotani, H. T. Yuan, M. Kawasaki, Y. Iwasa, *Appl. Phys. Lett.* **2010**, *97*, 142110.
[25] W. Dou, J. Sun, J. Jiang, A. Lu, Q. Wan, *Jpn. J. Appl. Phys.* **2010**, *49*, 110201.
[26] Y. Yamada, K. Ueno, T. Fukumura, H. T. Yuan, H. Shimotani, Y. Iwasa, L. Gu, S. Tsukimoto, Y. Ikuhara, M. Kawasaki, *Science* **2011**, *332*, 1065.
[27] M. Dai, W. Xu, *Appl. Phys. Lett.* **2012**, *100*, 113506.
[28] J. T. Ye, S. Inoue, K. Kobayashi, Y. Kasahara, H. T. Yuan, H. Shimotani, Y. Iwasa, *Nat. Mater.* **2010**, *9*, 125.
[29] H. T. Yuan, M. Toh, K. Morimoto, W. Tan, F. Wei, H. Shimotani, Ch. Kloc, Y. Iwasa, *Appl. Phys. Lett.* **2011**, *98*, 012102.
[30] K. Taniguchi, A. Matsumoto, H. Shimotani, H. Takagi, *Appl. Phys. Lett.* **2012**, *101*, 042603.
[31] F. Wang, M. E. Itkis, R. C. Haddon, *Nano Lett.* **2010**, *10*, 937.
[32] F. Wang, M. E. Itkis, E. Bekyarova, R. C. Haddon, *Nat. Photonics* **2013**, *7*, 459.
[33] Z. Wu, Z. Chen, X. Du, J. M. Logan, J. Sippel, M. Nikolou, K. Kamaras, J. R. Reynolds, D. B. Tanner, A. F. Hebard, A. G. Rinzler, *Science* **2004**, *305*, 1273.
[34] J. Kong, E. Yenilmez, T. W. Tombler, W. Kim, H. Dai, *Phys. Rev. Lett.* **2001**, *87*, 106801.
[35] M. P. Anantram, T. R. Govindan, *Phys. Rev. B* **1998**, *58*, 4882.
[36] K. Yanagi, R. Moriya, Y. Yomogida, T. Takenobu, Y. Naitoh, T. Ishida, H. Kataura, K. Matsuda, Y. Maniwa, *Adv. Mater.* **2011**, *23*, 2811.
[37] R. Landauer, *Philos. Mag.* **1970**, *21*, 863.
[38] J.-C. Charlier, X. Blase, S. Roche, *Rev. Mod. Phys.* **2007**, *79*, 677.
[39] D. Yu, C. Wang, P. Guyot-Sionnest, *Science* **2003**, *300*, 1277.
[40] K. Yanagi, H. Udoguchi, S. Sagitani, Y. Oshima, T. Takenobu, H. Kataura, T. Ishida, K. Matsuda, Y. Maniwa, *ACS Nano* **2010**, *4*, 4027.
[41] X. Liu, T. Pichler, M. Knupfer, M. S. Golden, J. Fink, H. Kataura, Y. Achiba, *Phys. Rev. B* **2002**, *66*, 045411.
[42] T. Ando, *J. Phys. Soc. Jpn.* **1997**, *66*, 1997.
[43] Y. Yomogida, J. Pu, H. Shimotani, S. Ono, S. Hotta, Y. Iwasa, T. Takenobu, *Adv. Mater.* **2012**, *24*, 4392.
[44] G. A. Snook, A. S. Best, A. G. Pandolfo, A. F. Hollenkamp, *Electrochem. Commun.* **2006**, *8*, 1405.